Design of a 5 : 1 Bandwidth Stripline Notch Array from FDTD Analysis

Mark Kragalott, *Member, IEEE*, William R. Pickles, *Member, IEEE*, and Michael S. Kluskens, *Member, IEEE*

***Abstract*—A 5 : 1 bandwidth stripline notch array antenna is designed from parametric investigations of flare and feed dimensions. The finite-difference time-domain (FDTD) method is employed to perform the parametric studies. Both linear and planar single-polarization arrays are considered with half-wavelength element spacing at the highest frequency. The linear-array elements depend upon *E*-plane element mutual coupling to achieve wideband behavior. Edge elements, which cannot benefit from full *E*-plane coupling, are shown to maintain good transmit performance with the application of amplitude tapering. The planar array is shown to have a scannability (active VSWR <2) averaging 51° off broadside in the *E*-plane and exceeding 60° in the *H*-plane. As an infinite planar array, the antenna is predicted to have a bandwidth exceeding 7 : 1 on broadside. Measurements are in good agreement with the computations.**

***Index Terms*—Element coupling, FDTD, phased arrays, stripline antenna, wide-band arrays.**

I. Introduction

ULTRAWIDE-BAND (UWB) array antennas are utilized for electronic steering applications requiring either multiple functions spanning a wide frequency range or pulse excitations. Traditionally, wide-band flared-notch antennas and arrays have been primarily analyzed through experimentation [1], [2], while in recent years, these antennas have been increasingly designed and analyzed using computational electromagnetics [3]–[5]. Assuming large periodic arrays with a substantial number of elements so that edge effects are negligible, many of these numerical array analyses are efficiently conducted on a unit cell of the array using periodic boundary conditions. Periodic boundary conditions, which simulate an infinite array, are satisfied either through the summation of Floquet modes [4], [6] or through numerical waveguide simulators [7]. Time-domain waveguide simulators, while not as versatile as full Floquet-mode solutions, offer a simple way of obtaining wide-band infinite planar array impedance from the computation of voltage and current followed by a Fourier transform. Since infinite-array analysis combines the mutual coupling effects of all array elements, finite-array analysis must be employed to predict the performance impact of coupling from individual elements. In addition, edge effects are most accurately predicted from the analysis of finite arrays.

In this paper, the active impedance of a stripline notch array is optimized over a 5 : 1 bandwidth for scan angles averaging at least 50° in both the *E*- and the *H*-plane. Achieving an active array voltage standing wave ratio (VSWR) of less than two over the required scan angles and operational frequencies assures scannability, while avoiding grating lobes when scanning to the horizon is enforced by half-wavelength element spacing at the highest frequency of operation. The finite-difference time-domain (FDTD) [8], [9] method is employed to optimize the feed and flare parameters of the array. Section II addresses the design procedure. In Section II-A, the stripline to slotline transition is optimized for good energy transfer across the frequency band. Section II-B describes the basis for employing active scan impedance optimization instead of element pattern optimization in the design process. In addition, the procedure for finding active scan impedance is described. In Section II-C, the optimal flare length element for a linear array is found. The linear array *E*-plane scan performance of the element is characterized in Section II-D and the effects of mutual coupling are analyzed. Section II-E presents the scan performance of planar arrays from FDTD numerical waveguide simulators. A numerical four-wall waveguide simulator is utilized to calculate the infinite planar-array broadside scan performance, and parallel-plate waveguide simulators are employed to examine *E*- and *H*-plane scan performance of planar arrays that are of infinite extent in one dimension. Finally, Section II-F describes the construction and measurement of linear and planar arrays for performance verification.

II. Design of the Stripline Notch Array

A linearly polarized wide-scan array is required that will operate over a frequency range of 1–5 GHz and wide scan angles without grating lobes. The printed stripline notch is chosen as the basic element because it offers directive wide-band behavior, repeatability in construction, and a low cross-polarization field component. The substrate dielectric selected is low-loss Duroid 5870 ($\epsilon_r = 2.33$, $\tan\delta = 0.0012$ @ 10 GHz) owing to its availability and ability to handle reasonable power levels without bonding failure. The thickness of the element is 0.157 cm ($0.0262\lambda_h$, where λ_h is the wavelength at 5 GHz)[1] from groundplane to groundplane. Thicker commercially available substrates were evaluated, but resulted in narrower array bandwidths. The exploded view of the array element in Fig. 1(a) shows that the element is comprised of two outer groundplane layers that are separated from the strip layer

Manuscript received April 7, 1999; revised March 31, 2000. This work was supported by the Office of Naval Research, Washington, D.C.

The authors are with the Naval Research Laboratory, Washington, DC 20375 USA.

Publisher Item Identifier S 0018-926X(00)07713-9.

[1]In this paper, element dimensions will be given primarily in terms of λ_h, which is the free-space wavelength of 0.06 cm at the highest frequency of 5 GHz. To find the element dimension in terms of λ_ℓ, which is the free-space wavelength at the lowest frequency of 1 GHz, the reader should divide the value in terms of λ_h by 5.

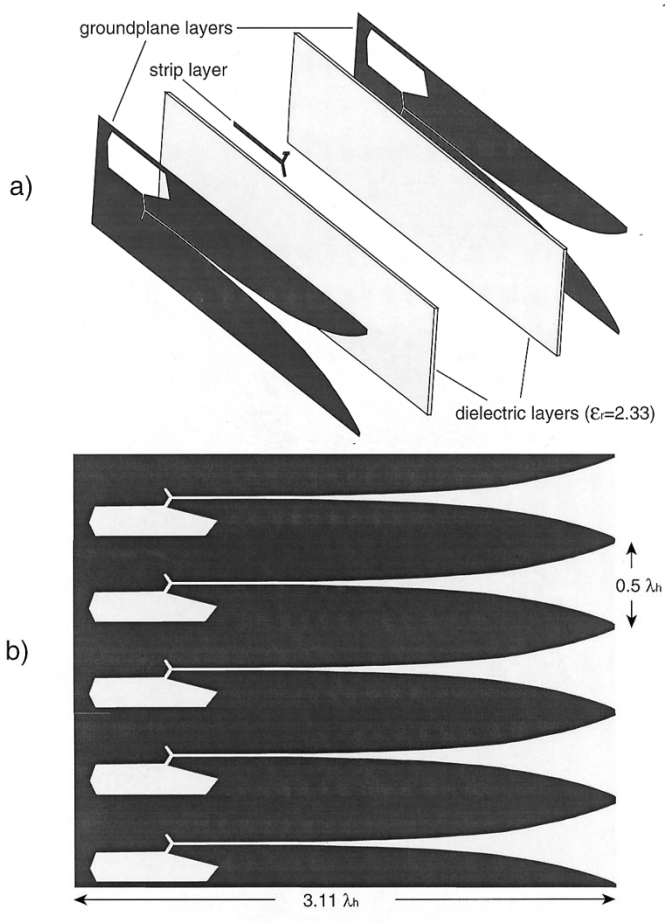

Fig. 1. (a) Exploded view of the stripline notch element and (b) linear array of 5 elements.

by two dielectric layers. The groundplane layers contain the slot and flare whereas the strip is electrically connected to the center conductor of a feeding coaxial line.

A. YY Stripline-to-Slotline Transition Design

The first issue to resolve is the manner of coupling wide-band energy from the stripline to slotline. The YY transition [10] pictured in Fig. 2(a) is utilized for this purpose owing to its good UWB behavior as noted in [11]. While previously described as a microstrip to slotline transition, extending the idea to stripline is natural. In this case, 0.119-cm ($0.0198\lambda_h$) wide 50-Ω stripline is employed because a 50-Ω coax TEM mode will couple readily to it. A slotline width of 0.0275 cm ($0.0046\lambda_h$) is chosen to produce a frequency averaged 50-Ω transmission line for impedance matching. The FDTD cell size is set equal to the slotline width, which makes the number of cells per free-space wavelength equal to 218 at the highest frequency of 5 GHz. The YY transition works as a six-port network that depends upon electrically short and geometrically opposed Y-arms, with one stripline Y existing in the strip layer and the oppositely oriented slotline Y present in each groundplane layer. Each Y contains a short circuit on one arm of the Y and an open circuit on the other arm. The propagation constants for both the stripline and slotline, which depend on the line effective dielectric constants, must be calculated because the electrical lengths of the Y-arms in the strip layer and the groundplane layer must be equivalent. In this case, the slotline propagates a quasi-TEM mode whose effective dielectric constant declines gently with frequency, whereas the stripline propagates a TEM mode whose effective dielectric constant is nearly constant with frequency. Therefore, the equivalent electrical length condition can only be satisfied in an average sense over the frequency range of the array. The FDTD calculated propagation constants dictate that the slot Y-arm should be a factor of 1.206 longer than the strip Y-arm. The slotline Y-arm is set at $0.06\lambda_h$ long, which requires that the stripline Y-arm length should be $0.0498\lambda_h$. However, the $0.0046\lambda_h$ FDTD cell size means that the Y-arm length ratios can only be approximated to within 4%. The stripline Y-arm short circuit is formed with a plated-through hole from the truncated strip end to each groundplane layer. The stripline Y-arm open circuit is formed in the usual manner by truncating the strip. The slotline short circuit in the groundplane layer is formed by a slot truncation. The largest obstacle to an effective YY transition design is the formation of a slotline open circuit. In principle, an open circuit is formed by truncating the slot into open dielectric. However, in practice, the open dielectric must be approximated by a finite-size cavity. Factors that limit the size of this cavity include the inter-element spacing, the position of the YY transition, and the length of the element. In addition, if dual polarization is planned, the cavity must accommodate orthogonal element insertion.

The groundplane layer cavity was numerically optimized without the flare attached. The slot is more than a wavelength long at the lowest UWB frequency with the open end of the slot terminated in FDTD absorbing boundary layers to simulate infinite length when testing the transition alone. A hexagonal cavity shape is used to simplify both modeling and modification. The VSWR of the YY transition for various groundplane layer cavity shapes and sizes is shown in Fig. 2(b). The cavity shapes are shown to scale relative to one another. It can clearly be seen that transitions with smaller cavities are less efficient at transferring lower frequency energy than larger cavities because the larger cavities are better approximations to an open circuit. For hexagonal cavities that are nearly circular in shape, only the largest cavity with an effective diameter of one half-wavelength at 5 GHz has acceptable behavior at frequencies near 1 GHz. However, this large cavity size is not acceptable if an orthogonal polarization element is to be inserted between the flares because the orthogonal element would intersect the cavity. The cavity design was optimized with the constraint to allow for a second polarization. The cavity shape that gives the best wide-band performance for the imposed constraints is shown in Fig. 2(a) and (b). The cavity area is increased over nearly circular hexagonal shapes through the elongation of the cavity in both the coaxial feed and flare directions. As observed in Fig. 2(a), the portion of the cavity sloping away from the slotline is a consequence of accommodating the stripline short circuit. It is important to note that avoiding this slope by looping around the short circuit causes no increase in bandwidth and that removing the

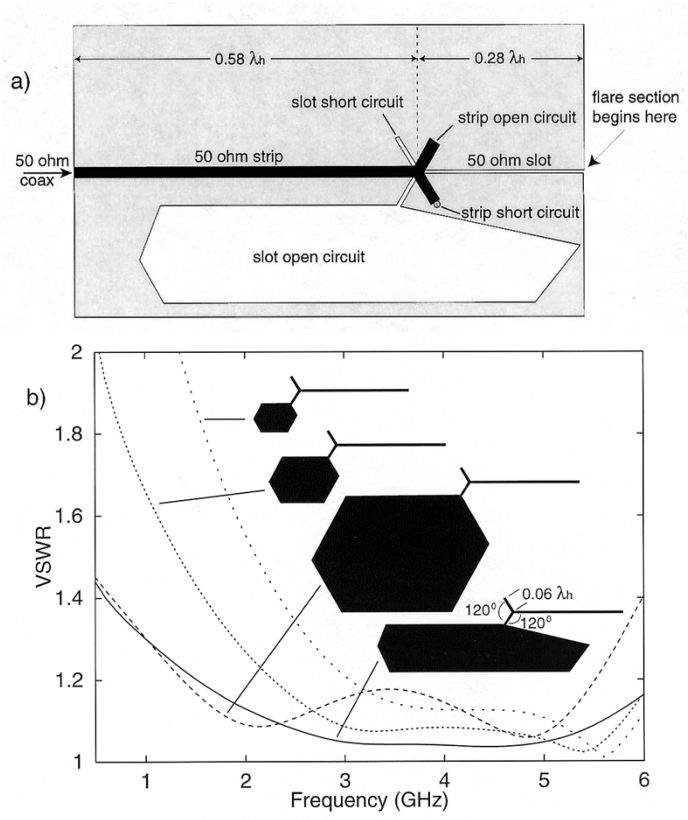

Fig. 2. (a) Detail of the YY transition and (b) calculated VSWR of various cavity sizes and shapes.

sharp cavity vertices with shaping gives very little performance change.

B. Active Reflection Coefficient and Element Pattern

Active impedance and far-zone patterns are vital performance measures for any array. Active impedance is a straightforward calculation of voltage and current in FDTD. In contrast, the far-zone pattern calculation is a computationally intensive operation in a standard FDTD solution. Fortunately, pattern calculation is not necessary in the array design procedure owing to the relationship between embedded element pattern and active impedance for large arrays. When a large planar array has no grating lobes in its pattern, the active array reflection coefficient $\Gamma(\theta, \phi)$ is approximately related to the normalized array element power pattern $P(\theta, \phi)$ in a terminated array environment [12], [13] by

$$|\Gamma(\theta, \phi)| = \sqrt{1 - \frac{\lambda^2 P(\theta, \phi)}{d_x d_y \cos\theta}} \tag{1}$$

where d_x and d_y are the element spacing in x and y, and (θ, ϕ) are standard spherical coordinates. In (1), $\theta = 0$ at broadside and the second term inside the square root never exceeds one since

$$P(\theta, \phi) \leq \frac{d_x d_y \cos\theta}{\lambda^2} \tag{2}$$

gives a upper bound on the terminated array element power pattern. Similar relationships hold for linear arrays. The implication of (1) is that if the active reflection coefficient (and thus, active VSWR) is low at a scan angle, then it is possible to scan with reasonable directive gain at that angle. Pattern calculations are thus not necessary in the design process since optimization of the active scan impedance assures scannability if thermal losses are small.

The active scan impedance of a finite array can be found over the full bandwidth and all angles by calculating the driven response of each antenna element with all other elements in the array terminated in matched loads. Linear superposition is then applied to obtain the active array impedance. For example, for a three element array with feed voltages of V_1, V_2, V_3 and feed currents of I_1, I_2, I_3, the relationship between the feed voltages and currents is given by

$$\begin{bmatrix} Y_{11} & Y_{12} & Y_{13} \\ Y_{21} & Y_{22} & Y_{23} \\ Y_{31} & Y_{32} & Y_{33} \end{bmatrix} \begin{bmatrix} V_1 \\ V_2 \\ V_3 \end{bmatrix} = \begin{bmatrix} I_1 \\ I_2 \\ I_3 \end{bmatrix}. \tag{3}$$

The admittance matrix $\mathbf{Y}$ is obtained by individually feeding each element n with the testing voltage $\tilde{V}_n$ and calculating the feed currents with all other feed voltages set to zero. Then the elements of the nth column of the admittance matrix are given by

$$Y_{mn} = \frac{I_m}{\tilde{V}_n} \tag{4}$$

for $m = 1, 2, 3$. To calculate the active impedance of an element at a given scan angle (θ, ϕ), the feed voltages for the phased array are given by

$$V_n = e^{-jk[(x_n \cos\phi + y_n \sin\phi)\sin\theta + z_n \cos\theta]} \tag{5}$$

where k is the wavenumber and (x_n, y_n, z_n) are the coordinates of each element. Then the active impedance is

$$Z_n = \frac{V_n}{I_n} = \frac{V_n}{Y_{n1}V_1 + Y_{n2}V_2 + Y_{n3}V_3}. \tag{6}$$

Using this postprocessing technique, the effects of nonuniform amplitude weighting on active impedance as well as edge effects in phased arrays can be studied without recalculating the FDTD response of the array for each set of parameters.

C. Optimal Linear Array Flare Length

The flare attaches to the YY transition section in a linear array configuration as shown in Fig. 1(b), and the scan impedance is numerically optimized by varying flare parameters. A seven element linear array is chosen to give the array an aperture width of greater than a half-wavelength at the lowest frequency of 1 GHz. The spacing between the elements is set at a half-wavelength at 5 GHz. A standard exponential taper is employed owing to its straightforward implementation, although other smooth tapers were successfully applied. The staircase approximation to the flare inherent with the orthogonal coordinate FDTD is not an issue owing to the very small cell size and the avoidance of half-wavelength long steps along the flare [14]. For a fixed aperture width, a short array element is preferable to a long one owing to its smaller size and wider embedded *E*-plane element pattern. Thus, the flare length was initially set at $0.25\lambda_h$, where

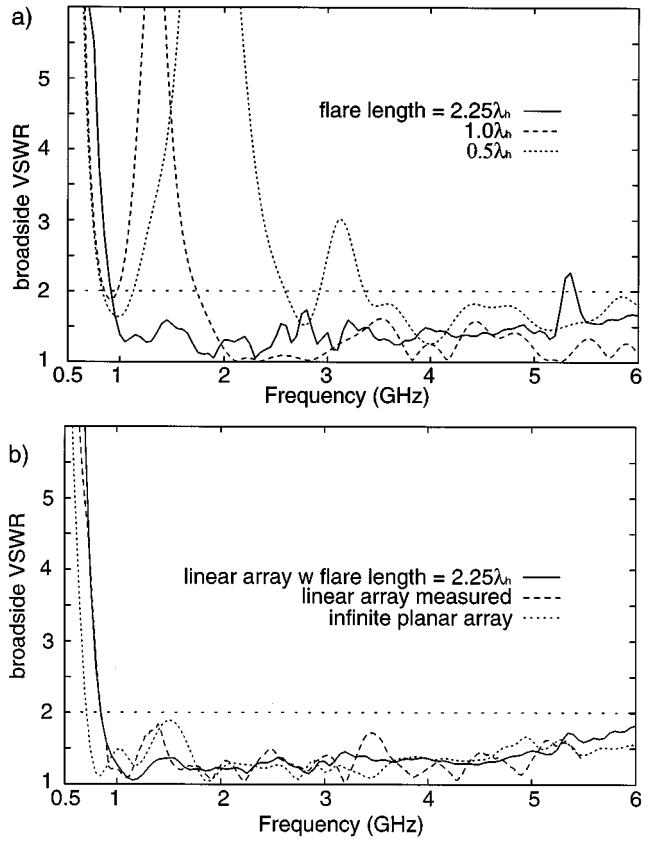

Fig. 3. (a) Calculated broadside scan VSWR of 7-element linear array for various flare lengths and (b) measured versus calculated broadside VSWR of an 8-element linear array and the infinite planar array VSWR.

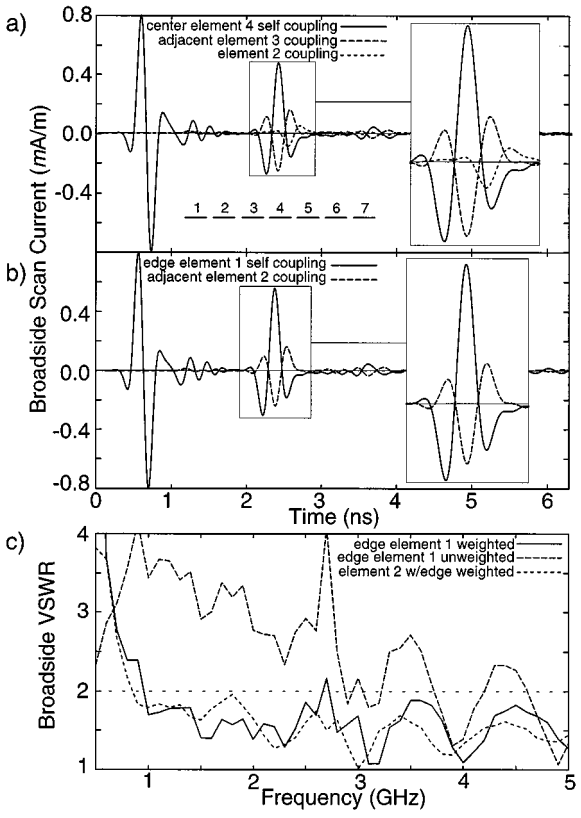

Fig. 4. (a) Calculated time-domain current coupling at the center element of a 7-element linear array; (b) calculated coupling at the edge element of the array; and (c) calculated broadside scan VSWR at the edge element for weighted versus unweighted sources.

λ_h is the free space wavelength at 5 GHz. However, this length gave an unacceptable center element broadside active VSWR over the entire frequency band. As a consequence, the flare was lengthened to $0.5\lambda_h$ and the acceptable broadside impedance improved down to 3.4 GHz as shown in Fig. 3(a). At $1.0\lambda_h$ flare length, the linear array had acceptable VSWR down to 1.8 GHz, but below that quickly rose to a large local VSWR maximum exceeding 6 near 1.6 GHz. This local VSWR maximum is attenuated by increasing the length further as indicated by the $2.25\lambda_h$ flare length curve, where the local VSWR maximum has been reduced to 1.6. Further, the acceptable broadside low frequency scan behavior has been reduced to 0.9 GHz. The flare length of $2.25\lambda_h$ ($0.45\lambda_l$) has achieved a broadside scan 5 : 1 impedance bandwidth. Increasing the flare length further has little benefit for the parameters examined. As seen in Fig. 3(b), a measurement of the constructed corporate fed 8-element linear array is compared against the calculated result, and good agreement is demonstrated.

D. Beneficial E-Plane Mutual Coupling in the Linear Array

To better understand the broadside wide-band active impedance behavior of the linear array, it is instructive to study the time-domain mutual coupling between elements of a seven element linear array when all elements are excited with equal amplitude and phase. The excitation pulse is a

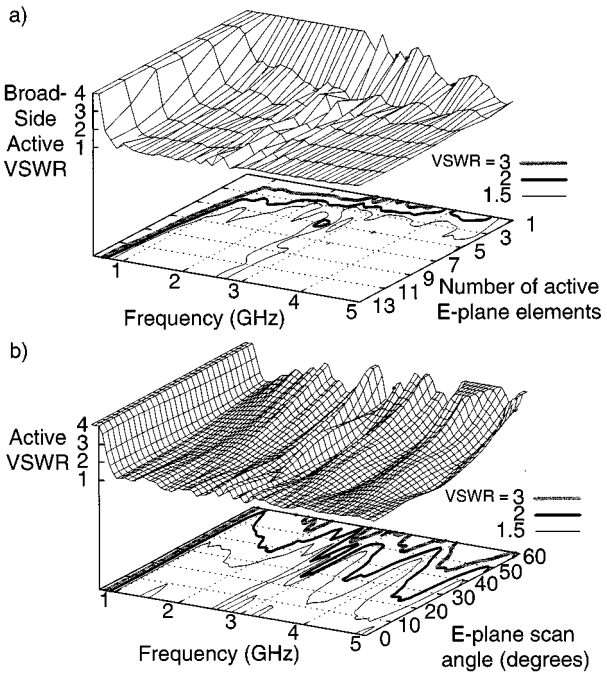

Fig. 5. (a) Calculated broadside scan VSWR of a 13-element linear array for various numbers of active elements and (b) calculated *E*-plane scan VSWR of the 7-element linear array.

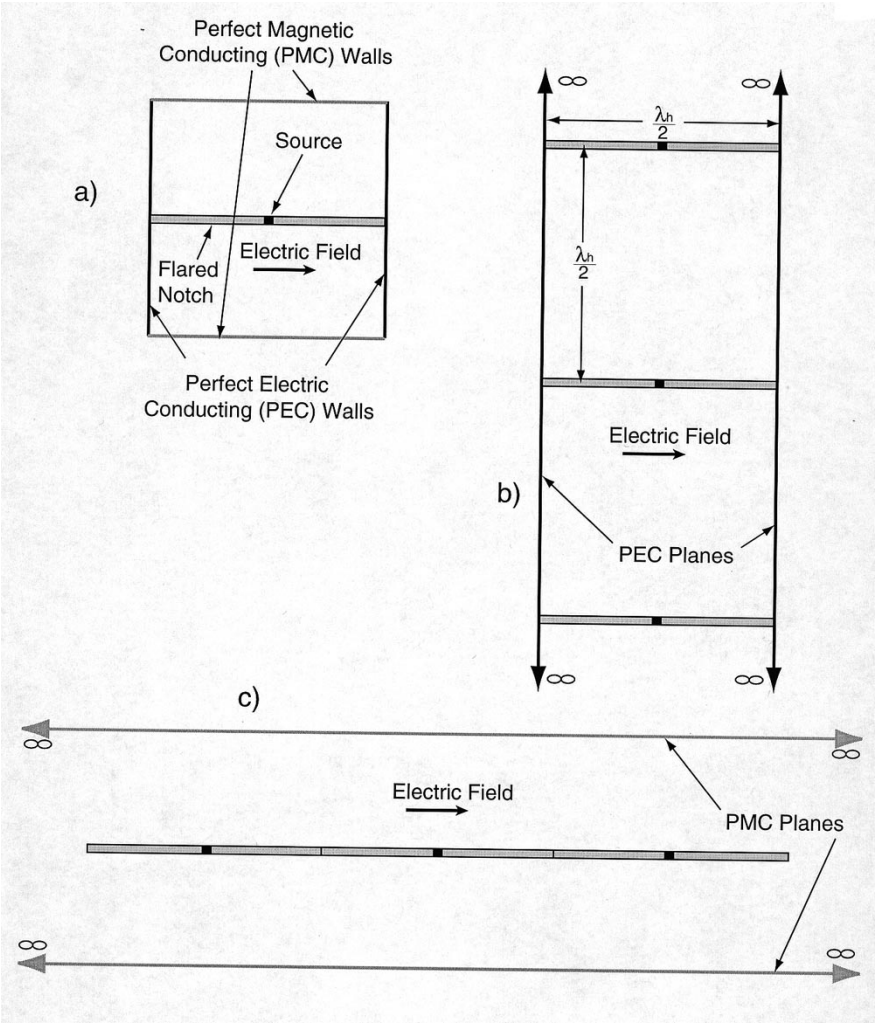

Fig. 6. (a) Broadside scan infinite planar array numerical waveguide simulator; (b) *H*-plane scan 3 row by infinite number of elements per row waveguide simulator; and (c) *E*-plane scan 3 elements per row by infinite number of rows waveguide simulator.

modulated Gaussian sine with more than 99% of the pulse energy contained between 0.75–5.25 GHz. Fig. 4(a) shows the time-domain current induced at the array center element 4 feed port due to itself, coupling from adjacent element 3, and coupling from element 2. Elements 5, 6, and 7 produce essentially the same amplitude and time phase current and voltage signal at element 4 as elements 3, 2, and 1, respectively. The self-coupling current in the first nanosecond strongly resembles the input current. In the highlighted time zone between 2–3 nanoseconds, the self-coupling current is indicative of strong aperture reflection owing to an aperture width less than a half-wavelength for frequencies below 5 GHz. However, the active element VSWR is excellent primarily because elements 3 and 5 provide nearly identical signals at port 4 that combine to cancel most of the aperture reflection of element 4. The energy is radiated since the effective aperture size has increased from the cooperation of active elements. The dominant portion of the remaining reflected voltage and current at element 4 is cancelled by elements 2 and 6. Elements 1 and 7 couple very weakly to element 4 except at the lowest frequencies, where residual element 4 aperture reflections are further cancelled to extend the impedance match to lower frequencies.

The beneficial *E*-plane mutual coupling effects of adjacent elements brings into question element performance at an edge element or next to a dormant element where the benefit of active array cancellation of aperture reflection is diminished. However, transmit power tapering can mitigate elevated VSWR at these elements. To demonstrate this principle, consider the case where the array is transmitting equal time phase and amplitude pulses on elements 1–7. Element 1 is an edge element with elements on only one side of it providing cancellation of its aperture reflection. The VSWR of element 1 under these conditions is shown in Fig. 4(c). It can clearly be seen that the VSWR of element 1 is elevated relative to a center element with all elements excited as seen in Fig. 3(a). Inspection of the highlighted time zone between 2 and 3 nanoseconds in Fig. 4(b) reveals that if the element 1 pulse amplitude is halved, element 2 would provide most of the cancellation required. Thus, as the simplest example of tapering the current and voltage of the incident pulse at elements 1 and 7 are weighted by one half, whereas the incident pulses of elements 2–6 remain unweighted. The diminished VSWR of the weighted edge element is contrasted with the unweighted edge element in Fig. 4(c). When the edge element is weighted, the adjacent unweighted element 2 will suffer a slightly elevated

VSWR owing to the imbalance of amplitude excitations of adjacent elements 1 and 3, but this elevation is small and could be mitigated with the incorporation of more sophisticated tapers. It should be noted that if there is a passively terminated edge element so that the first active element is the second element, then amplitude tapering performed on this second element is considerably more effective than the case considered above.

Fig. 5(a) shows the broadside scan VSWR of a 13-element linear array as a function of the number of active elements. The first active element is the center element with all other elements terminated in 50-Ω loads. Successive pairs of elements on either side of the center element are made active to form the contour plot. The single active element VSWR is quite poor because adjacent element coupling is required to cancel the aperture reflection. The single active element VSWR calculation is confirmed with good accuracy against measurements. At least seven active elements are required to get adequate 5 : 1 bandwidth behavior, but the low frequency impedance match is shown to improve as the number of active elements continues to increase toward 13. Notice that the rate of low frequency performance improvement declines with increasing elements. This is most likely the result of feed limitations as the YY transition open circuit cavity becomes electrically smaller with decreasing frequency. The broadside scan bandwidth of a 13-active-element linear array is 7 : 1.

The active scan VSWR performance of the seven-element linear array in the *E*-plane as function of frequency and scan angle is shown in Fig. 5(b). It can be seen that *E*-plane scan performance is good across the 5 : 1 bandwidth for scan angles up to an average of 45°. As the frequency increases, there are narrowed scan regions at some frequencies. Fig. 4(a) helps to illustrate that when signals are fed in time phase, as they are in the broadside scan case, neighboring *E*-plane element coupling tends to cancel the aperture reflection of an element. When time-delay steering is employed, signal cancellation deteriorates owing to divergent time phasing of elements. This effect tends to worsen with increasing scan angle, and thus frequency averaged VSWR also rises with scan angle. In all contour plots presented in this paper, the active scan VSWR is nearly symmetric about broadside scan, so only half the scan volume is plotted.

E. Planar Array Scan Analysis with Numerical Waveguide Simulators

Planar array scan performance is characterized by adding multiple rows of elements with the aid of computationally efficient numerical waveguide simulators. A single row is defined by a linear array of elements in the *E*-plane. Each row is separated from the adjacent row by half-wavelength spacing at 5 GHz. Initially, the infinite planar array performance is characterized in a FDTD broadside scan four wall waveguide simulator [7] holding a single element as shown in Fig. 6(a). The simulator is comprised of two magnetic conducting plates parallel to the *E*-plane placed above and below the element at a distance of one half the element spacing and two electric conducting plates parallel to the *H*-plane placed at the element edges. The waveguide simulator is terminated in FDTD absorbing boundary layers to simulate infinite length. The broadside VSWR of the infinite planar array is shown in Fig. 3(b). The broadside scan bandwidth of the planar array is 7 : 1 since the active VSWR is less than 2 for frequencies down to 0.75 GHz. The infinite planar array exhibits a local VSWR maximum of 1.95 between 1 and 2 GHz. As in the linear array case, the planar array active VSWR rises for lower frequency ranges if the flare length is shortened from $2.25\lambda_h$. The broadside scan VSWR predicts that good performance is to be expected if the array is very large. Owing to the large resource requirements imposed by both the small FDTD cell size (218 cells per free space wavelength at 5 GHz) and large planar arrays, numerical infinite parallel plate waveguide simulators were employed to analyze semi-infinite planar array scan behavior.

For efficient calculation of *E*-plane scan VSWR, infinite magnetic conducting plates parallel to the *E*-plane are placed both above and below a 7-element linear array at a distance of one half the element spacing. This arrangement simulates a planar array with seven elements per row and an infinite number of rows. Fig. 6(c) illustrates a similar type of *E*-plane simulator with three elements per row. By phasing the elements, scan performance in the *E*-plane can be found. Analysis of the mutual coupling indicates that the best performance is obtained when edge element sources are amplitude weighted by one half, whereas all other sources have unit amplitude weights. Fig. 7(a) shows the *E*-plane scan performance of the array. With the exception of a small scan region near broadside between 1.3–1.6 GHz where the active VSWR slightly exceeds 2, scan performance is good down to 0.75 GHz and up to 5 GHz for scan angles up to an average of 51°. The infinite planar array broadside scan curve in Fig. 3(b) clearly shows that the VSWR between 1.3–1.6 GHz will decline below 2 as the number of *E*-plane elements increases. However, the computational resources required to find this limit were not available.

In the *H*-plane scan case, infinite electric conducting plates parallel to the *H*-plane are positioned on each edge of five vertically stacked single-element rows. This simulates a planar array that has five rows with an infinite number of elements per row. Fig. 6(b) illustrates a similar type of *H*-plane simulator with three rows. Scan performance in the *H*-plane can be found with the phasing of each row. Fig. 7(b) shows that the *H*-plane scannability of the array extends from 1 to 5 GHz and includes nearly all angles out to 60°. The planar-array broadside scan VSWR curve in Fig. 3(b) shows that the array will operate significantly below 1 GHz as the number of rows increases to some undefined limit. Again, limited computational resources prevented the discovery of this limit. Fig. 7(c) shows how the number of active rows in a 5-row environment impacts broadside scan VSWR. A single active center row with the other rows terminated in 50-Ω loads has performance degradation relative to a single row in free space (linear array) shown in Fig. 3(b). Thus, the beneficial element to element coupling in the *E*-plane is negatively impacted by multiple bounces from the passive rows. This effect can be observed directly in time domain mutual coupling analysis. It is interesting to note in Fig. 7(c) that an even number of active rows, which corresponds to asymmetrical excitation, produces excellent *H*-plane performance. With three active rows, the VSWR

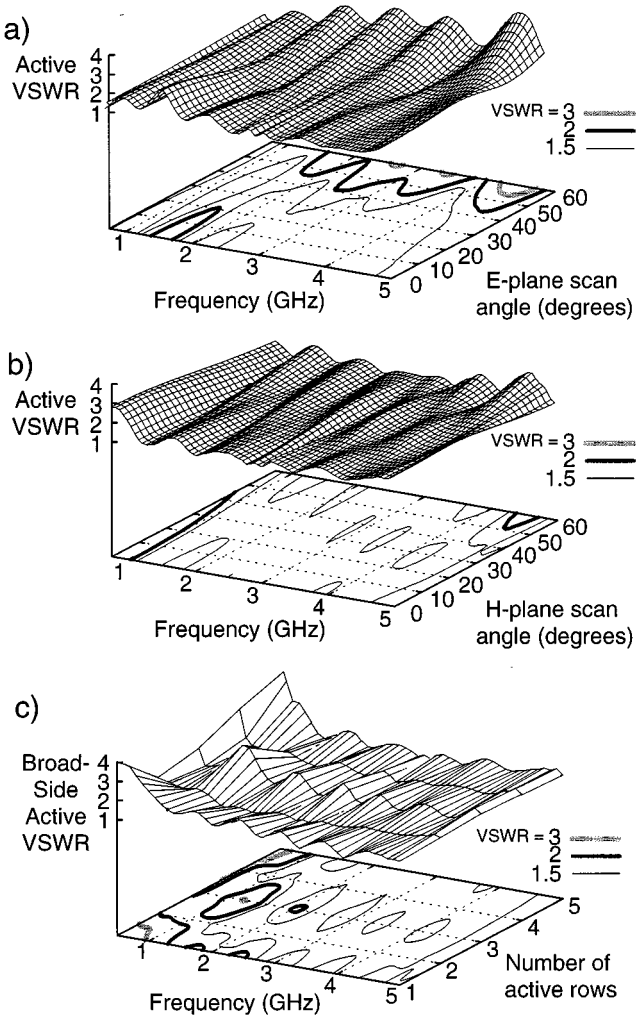

Fig. 7. (a) Calculated *E*-plane scan VSWR of a 7-element wide-planar array with an infinite number of rows; (b) calculated *H*-plane scan VSWR of a 5-row planar array with an infinite number of elements per row; and (c) calculated broadside scan VSWR of the 5-row semiinfinite planar array with various numbers of active rows.

exceeds 2 in two low-frequency ranges, but when the number of active rows is increased to 5, the broadside scan VSWR remains below 2 from 1 to 5 GHz.

F. Constructed Planar Array Pattern and Active VSWR Measurements

A single polarization 8 × 8 planar array was constructed and measured both to verify the scan impedance performance of the numerical array design and to characterize the patterns. A given row was fed by a coaxial line through a corporate feed network. The measured co-pol array gain patterns in the *E*-plane and *H*-plane for broadside scan are shown in Fig. 8 from 1 to 5 GHz along with the co-pol element patterns and the cross-pol array patterns. No amplitude tapering was applied to the array. The co-pol gain increases from approximately 9 dBi near 1 GHz to 20 dBi near 5 GHz. Naturally, the beamwidth of the pattern declines with increasing frequency owing to the increasing gain. The arrays were also successfully scanned to 50° in the both the *E*-plane and *H*-plane using time-delay networks. Depending on the frequency, the co-pol gain at 50° scan in the *E*-plane and

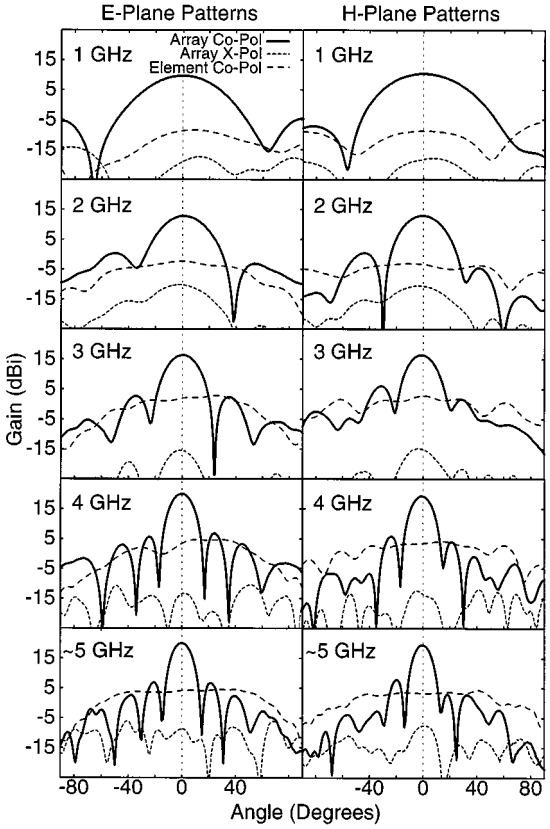

Fig. 8. Measured cross-pol and co-pol patterns of an 8 × 8 planar array for broadside scan and the center element co-pol pattern.

H-plane varies from 2 to 4 dB lower than the broadside scan co-pol gain. From 1 to 5 GHz, the broadside scan cross-pol of the array is down by an average of 28 dB from the co-pol, and averages 20 dB down for 50° *E*-plane and *H*-plane scans. The aperture efficiency of the array, which is defined by the ratio of maximum effective aperture to the physical aperture size, averages 62% from 1 to 5 GHz on broadside scan, although the antenna is more efficient at lower frequencies. The front to back ratio on broadside scan ranges from approximately 20 dB at the low frequency to 30 dB at the high frequency.

The measured and calculated active VSWR of the array at broadside scan are compared in Fig. 9(a). The same comparison is made for the active VSWR at 50° *E*-plane scan in Fig. 9(b) and for 50° *H*-plane scan in Fig. 9(c). The curves show good agreement considering the complexity of the antenna and the subtle differences between the constructed elements and the FDTD simulated elements. In addition, the measurements employ a corporate feed that combines all signals from a row or column of elements back at the receiver, whereas the calculations assume a transmit and receive module at each element. Further, the 8 × 8 constructed array is too large a problem to be handled by present computational resources, so the numerical arrays are semiinfinite. This can cause differences in active VSWR between the measured 8 × 8 array and the semiinfinite array because convergence of the solution is dependent on the number of active elements in each dimension as seen in Fig. 5(a) and Fig. 7(c). The biggest discrepancy between measurement and FDTD occurs in the 50° *E*-plane scan, where the measured

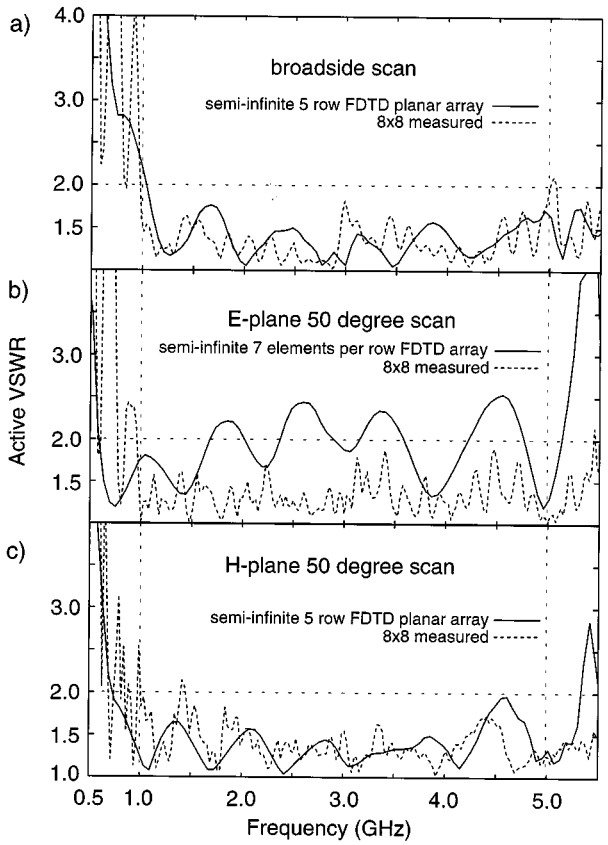

Fig. 9. Measured versus calculated VSWR of planar arrays at (a) broadside scan; (b) *E*-plane 50° scan; and (c) *H*-plane 50° scan.

VSWR has a lower value than the calculated VSWR over most of the 5 : 1 band. The discrepancy between the curves could be a result of numerical error arising from staircase approximations to the YY transition, but doubling the resolution of the FDTD grid to resolve the issue is not feasible with available computational resources. However, the desired 5 : 1 bandwidth behavior of the stripline notch array has been demonstrated.

III. Conclusion

A 5 : 1 bandwidth single-polarization stripline notch array has been designed from a combination of infinite and finite array FDTD analysis. The value of infinite array analysis is that good designs can be achieved with efficient use of resources. The drawback of such an approach is that mutual coupling effects are lumped together, thereby masking the beneficial or harmful effects of individual interactions within the array. Finite-array analysis, although more computationally intensive, permits the direct analysis of element interactions and thus facilitates the understanding and improvement of an array that may have been designed with infinite array techniques. Time-domain finite-array mutual-coupling analysis permits the evaluation of wide-band interactions within the array. In this case, time-domain analysis led to both the wide-band mitigation of linear-array edge-element reflections and the understanding of the beneficial effects of mutual coupling on the wide-band behavior of the array. A future paper will address the dual polarization case.

References

[1] P. J. Gibson, "The Vivaldi antenna," in *European Mic. Conf.*, 1979, pp. 101–105.
[2] M. J. Povinelli, "A planar broadband flared microstrip slot antenna," *IEEE Trans. Antennas Propagat.*, vol. 35, pp. 968–972, Aug. 1988.
[3] R. Janaswamy, "An accurate moment method model for the tapered slot antenna," *IEEE Trans. Antennas Propagat.*, vol. 37, pp. 1523–1528, Dec. 1989.
[4] D. H. Schaubert, J. A. Aas, M. E. Cooley, and N. E. Burris, "Moment method analysis of infinite stripline-fed tapered slot antenna arrays with a ground plane," *IEEE Trans. Antennas Propagat.*, vol. 42, pp. 1161–1166, Aug. 1994.
[5] E. Thiele and A. Taflove, "FDTD analysis of vivaldi flared horn antennas and arrays," *IEEE Trans. Antennas Propagat.*, vol. 42, pp. 633–641, May 1994.
[6] D. T. McGrath, "Periodic structure analysis using a hybrid finite element method," *Radio Science*, vol. 31, pp. 1173–1179, Sept. 1996.
[7] M. Gustavsson, J. Sanford, and M. Sundberg, "An analysis approach for large planar arrays using a bound FDTD model," in *URSI Int. Symp. Dig.*, July 1995, p. 5.
[8] K. S. Yee, "Numerical solution of initial boundary value problems involving Maxwell's equations in isotropic media," *IEEE Trans. Antennas Propagat.*, vol. 14, pp. 302–307, May 1966.
[9] R. J. Luebbers, *User's Manual for XFDTD*. State College, PA 16805: REMCOM, Inc., July 1994.
[10] B. Scheik and J. Kohler, "An improved microstrip-to-microslot transition," *IEEE Trans. Microwave Theory Tech.*, pp. 231–233, Apr. 1976.
[11] A. K. Lai, A. L. Sinopoli, and W. D. Burnside, "A novel antenna for ultra-wide-band applications," *IEEE Trans. Antennas Propagat.*, vol. 40, pp. 755–760, July 1992.
[12] W. Wasylkiwskyj and W. K. Kahn, "Element patterns and active reflection coefficient in uniform phased arrays," *IEEE Trans. Antennas Propagat.*, vol. 22, pp. 207–212, Mar. 1974.
[13] R. C. Hansen, *Microwave Scanning Antennas: Array Theory and Practice*. New York: Academic, 1966, vol. 2.
[14] K. L. Shlager, G. S. Smith, and J. G. Maloney, "Optimization of bow-tie antennas for pulse radiation," *IEEE Trans. Antennas Propagat.*, vol. 42, pp. 975–982, July 1994.

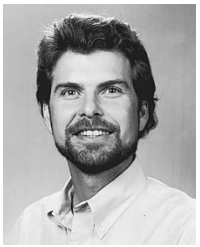

Mark Kragalott (S'89–M'00) received the B.A. degree in physics and economics at Kenyon College, Gambier, OH, in 1983 and the M.S. and Ph.D. degrees in electrical engineering from The Ohio State University, Columbus, OH, in 1988 and 1993, respectively.

From 1986 to 1993, he was a Graduate Research Associate at the ElectroScience Laboratory, Department of Electrical Engineering, The Ohio State University, where he conducted research on method of moments and extremely low frequency shielding. Since 1994, he has been with the Electromagnetics Section in the Analysis Branch of the Radar Division at the Naval Research Laboratory, Washington, DC. His research interests are in computational electromagnetics and ultrawide-band antennas and scattering.

William R. Pickles (S'87–M'87) received the B.S.E.E degree (with honors) from the University of California at Davis in 1980 and the M.S.E.E degree from the University of Wisconsin at Madison in 1987.

From 1980 to 1985 he was a Staff Engineer with the McDonnell Douglas Electro-Optics laboratory in Huntington Beach, CA. Since 1987, he has been with the Antenna Section of the Radar Division at the Naval Research Laboratory in Washington DC. His main area of research there has been in antennas, specifically in ultra wide-band flared notch antennas. In addition he has done work on the SPS-67 and SPS-49 radars and ultra-low sidelobe antennas.

Mr. Pickles is a member of Tau Beta Pi.

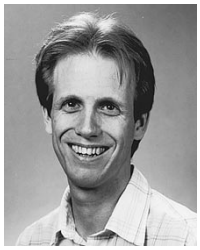

Michael S. Kluskens (S'81–M'91) received the B.S. and M.S. degrees in electrical engineering from Michigan Technological University, Houghton, MI, in 1984 and 1985, respectively, and the Ph.D. degree in electrical engineering from The Ohio State University, Columbus, OH, in 1991.

From 1986 to 1991, he was a Graduate Research Associate at the ElectroScience Laboratory, Department of Electrical Engineering, The Ohio State University, where he conducted research on method of moments and chiral media. He has been with the Radar Division of the Naval Research Laboratory, Washington, DC, since 1991 and is currently with the Electromagnetics Section in the Analysis Branch. His primary research interest is in computational electromagnetics with emphasis on method of moments, finite-difference time-domain, and radiation and scattering from large complex structures.